Inorganic Chemistry

pubs.acs.org/IC

Article

Near-Infrared-to-Near-Infrared Optical Thermometer BaY_2O_4: Yb^{3+}/Nd^{3+} Assembled with Photothermal Conversion Performance

Guotao Xiang,* Menglin Yang, Zhen Liu, Yongjie Wang, Sha Jiang, Xianju Zhou, Li Li, Li Ma, Xiaojun Wang,* and Jiahua Zhang*

Cite This: *Inorg. Chem.* 2022, 61, 5425−5432

Read Online

ACCESS | Metrics & More | Article Recommendations | Supporting Information

ABSTRACT: Nowadays, the construction of photothermal therapy (PTT) agents integrated with real-time thermometry for cancer treatment in deep tissues has become a research hotspot. Herein, an excellent photothermal conversion material, BaY_2O_4: Yb^{3+}/Nd^{3+}, assembled with real-time optical thermometry is developed successfully. Ultrasensitive temperature sensing is implemented through the fluorescence intensity ratio of thermally coupled Nd^{3+}: ^4F_j (j = 7/2, 5/2, and 3/2) with a maximal absolute and relative sensitivity of 68.88 and 3.29% K^{-1}, respectively, which surpass the overwhelming majority of the same type of thermometers. Especially, a thermally enhanced Nd^{3+} luminescence with a factor of 180 is detected with irradiation at 980 nm, resulting from the improvement in phonon-assisted energy transfer efficiency. Meanwhile, the photothermal conversion performance of the sample is excellent enough to destroy the pathological tissues, of which the temperature can be raised to 319.3 K after 180 s of near-infrared (NIR) irradiation with an invariable power density of 13.74 mW/mm^2. Besides, the NIR emission of Nd^{3+} can reach a depth of 7 mm in the biological tissues, as determined by an ex vivo experiment. All the results show the potential application of BaY_2O_4: Yb^{3+}/Nd^{3+} as a deep-tissue PTT agent simultaneously equipped with photothermal conversion and temperature sensing function.

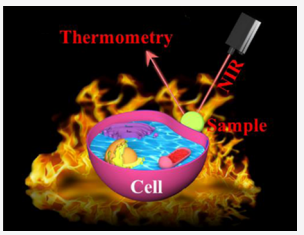

INTRODUCTION

In the 21st century, cancer has become one of the most serious public health problems faced by mankind. Clinical treatment methods such as surgical operations, chemotherapy treatments, and radiation therapy are inefficient due to their scarcity of selectivity to tumor cells or high toxicity and side effects. To overcome the abovementioned problems, photothermal therapy (PTT) is becoming a hot topic in scientific research, which refers to eliminating tumor cells through the thermal effect resulting from the energy precipitation in pathological tissues in some way. During the actual treatment process, the temperature of the lesion area should be controlled in a reasonable range to guarantee not only the effective ablation of the cancer cells but also the avoidance of damaging the surrounding normal tissues caused by the overheating effect.[1−5] Therefore, it is quite essential to develop an efficient and accurate method for temperature detection to serve PTT.

The temperature sensing behavior realized by the fluorescence intensity ratio (FIR) of thermal-coupled levels (TCLs) in rare earth ion-doped upconversion (UC) materials has the advantages of noncontact, high accuracy, short response time, large spatial resolution, and strong electromagnetic interference resistance, making it eminently suitable as a temperature sensor for the PTT process.[6−11] However, the current studies involved with FIR-based temperature measurement mainly focus on the green emission originating from the Er^{3+}: $^2H_{11/2}$/$^4S_{3/2}$ level, which owns excellent thermal coupling properties and temperature sensing performance.[12−16] Nevertheless, the shallow penetration depth of green light in the biological tissues caused by strong scattering and absorption phenomena seriously restricts the clinical application of Er^{3+}-based thermometric probes.[17−21] By comparison, the thermally coupled Nd^{3+}: ^4F_j (j = 7/2, 5/2, and 3/2) levels may be a perfect replacer for FIR-based temperature sensing, which can generate far-red and near-infrared (NIR) luminescence just by locating in the optical window of the biological tissue under the sensitization of Yb^{3+}.[14,22−26] Meanwhile, the much larger energy gap (ΔE) of the Nd^{3+}: $^4F_{7/2}$/$^4F_{3/2}$ level (~2000 cm^{-1}) than that of the Er^{3+}: $^2H_{11/2}$/$^4S_{3/2}$ level (~800 cm^{-1}) means that a much higher thermometric sensitivity can be achieved. In addition, the abundant metastable energy levels with small ΔE existing in Nd^{3+} ions can effectively convert part of the absorbed NIR light into thermal energy through nonradiative relaxation (NR) processes.[27] Therefore, it can be anticipated that the Yb^{3+}/Nd^{3+}-codoped system is an ideal PTT agent, integrating outstanding photothermal conversion ability with sensitive temperature detection operating in the biological window.[28−32]

Received: February 8, 2022
Published: March 25, 2022

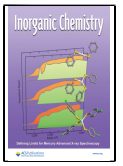

In the present paper, BaY_2O_4 is employed as the matrix material for doping Yb^{3+} and Nd^{3+}, which is an excellent host for the luminescence of rare earth ions and has good thermal stability.[33,34] An ultrasensitive temperature sensing along with the function of photothermal conversion is found in BaY_2O_4: Yb^{3+}/Nd^{3+}. The thermally enhanced mechanisms of Nd^{3+} luminescence along with the temperature sensing properties realized by the thermally coupled Nd^{3+}: ^4F_j (j = 7/2, 5/2, and 3/2) levels are investigated meticulously. Meanwhile, the photothermal conversion capacity of the synthesized material with the irradiation of NIR light is studied in detail. Beyond that, a simple ex vivo examination is performed to explore the penetration depth of the sample in the biological organism. All the data indicated that BaY_2O_4: Yb^{3+}/Nd^{3+} can be used as a new-type PTT agent possessing the ability of real-time temperature sensing.

EXPERIMENTAL SECTION

Chemicals. $BaCO_3$ (99.99%), Y_2O_3 (99.99%), Yb_2O_3 (99.99%), and Nd_2O_3 (99.99%) were supplied by Sinopharm Chemical Reagent Company of China, and all the chemical reagents were employed as the raw materials with no further purification.

Preparation. First, weigh the raw materials in stoichiometric proportion and then grind them in an agate mortar for 30 min. Second, the powder is transferred to a crucible with a lid for presintering in the muffle furnace at 600 degree centigrade for 6 h. Until cooled to the ambient temperature, the raw materials are taken out for a 30 min grind again. Finally, the powder is calcined for 6 h in the muffle furnace at 1300 degree centigrade.

Characterization. An XD-2 diffractometer produced by Beijing Persee is used to collect the powder X-ray diffraction (XRD) data. The spectroscopic data is detected using a FLS1000 model spectrometer made by Edinburgh Instruments Ltd. Meanwhile, a semiconductor laser with a wavelength of 980 nm is utilized as the excitation source for spectroscopic measurements. An HFS600E-PB2 temperature control device supplied by Linkam Scientific Instruments is employed to cooperate with the spectrometer for spectra collection at various temperatures. The lifetime values are obtained from the integral area of the corresponding normalized decay curves.

RESULTS AND DISCUSSION

Structure. The XRD patterns of Yb^{3+} and Nd^{3+}-codoped BaY_2O_4 with different concentrations are depicted in Figure 1. Notably, the information from the diffraction peaks of each sample, including relative intensities and locations, is in accordance with the standard XRD data of BaY_2O_4 (PDF#27-0044), indicating a complete insertion of Yb^{3+} ions and Nd^{3+} ions into the BaY_2O_4 lattice to form a solid solution construction. Moreover, no obvious shift of the diffraction peaks is detected due to the similar ionic radii of Y^{3+} (0.89 Å), Yb^{3+} (0.86 Å), and Nd^{3+} (1.00 Å).

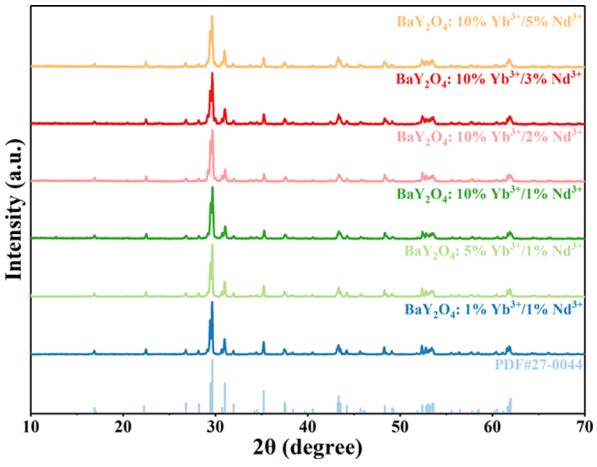

Figure 1. XRD patterns of BaY_2O_4: x % Yb^{3+}/y % Nd^{3+} (x = 1, 5, and 10; y = 1, 2, 3, and 5).

Luminescence Properties. Figure 2a,b displays the emission spectra of the as-prepared samples under the excitation of 980 nm wavelength. Three distinct emission bands appear in the range of 700−900 nm, which are attributed to Nd^{3+}: $^4F_{7/2} \rightarrow {}^4I_{9/2}$ at 752 nm, Nd^{3+}: $^4F_{5/2} \rightarrow {}^4I_{9/2}$ at 820 nm, and Nd^{3+}: $^4F_{3/2} \rightarrow {}^4I_{9/2}$ at 880 nm, respectively. The optimum doping concentrations of both Yb^{3+} and Nd^{3+} in the BaY_2O_4 host are determined to be 1% through a variable-controlling method, by which the strongest Nd^{3+} emission can be acquired. The overall luminescence intensity would be decreased when the doping concentration of Yb^{3+} or Nd^{3+} surpasses the abovementioned value due to the concentration quenching effect.

As shown in Figure 3a, two energy transfer (ET) routes can be involved in the Yb^{3+} and Nd^{3+} codoped system, including a single-photon process (ET1) and a two-photon process (ET2 and ET3). On the one hand, the excited Yb^{3+} can deliver its energy to the Nd^{3+} at the ground state through a phonon-assisted (PA) ET process, resulting in the population of the Nd^{3+}: $^4F_{3/2}$ state (ET1). On the other hand, the Nd^{3+} at the $^4I_{9/2}$ level can also receive energy directly from the excited Yb^{3+} to jump to the $^4I_{15/2}$ level (ET2) and then extract energy from another Yb^{3+} to populate to the $^2H_{11/2}$ level (ET3) followed by an NR process, giving rise to the population of the Nd^{3+}: $^4F_{3/2}$ state. It is important to point out that the excess energy deriving from the whole ET2 and ET3 processes is mainly transferred to heat via phonon vibrations.[35] Finally, the Nd^{3+} at the $^4F_{3/2}$ level can be further excited to the upper $^4F_{5/2}$ or $^4F_{7/2}$ level through the assistance of active lattice phonons because of their relatively small ΔE. In order to ulteriorly determine the the ET mechanisms of the Yb^{3+} and Nd^{3+} codoped system, the power density dependence of the emission intensity in BaY_2O_4: 1% Yb^{3+}/1% Nd^{3+} is measured and presented in Figure 3b. The relational expression of emission intensity (I) and power density (P) is written as $I \propto P^n$. Here, n denotes the NIR photon number that needs to be absorbed for emitting a high-energy photon, which can be obtained by the slope of the linear curve of $\log(I)$ and $\log(P)$. Excited by 980 nm, the n value of the $^4F_{5/2} \rightarrow {}^4I_{9/2}$ transition changes from 0.98 to 1.54 when the excitation power density exceeds 9.69 mW/mm^2, revealing that the single-photon process is dominant at the low excitation power density, and the two-photon process occurs and gradually increases with the rising excitation power density.

Thermally Enhanced Luminescence. Figure 4a shows the temperature-dependent spectra of BaY_2O_4: 1% Yb^{3+}/1% Nd^{3+} under the excitation of 980 nm wavelength, indicating that the emission intensity of the Nd^{3+}: ^4F_j (j = 7/2, 5/2, and 3/2) $\rightarrow {}^4I_{9/2}$ transition increases significantly with the rising temperature. This phenomenon can also be observed more intuitively from the digital photos of the far-red luminescence of the sample taken at 298 and 319 K, respectively, which is attributed to the band edge of the Nd^{3+}: $^4F_{7/2} \rightarrow {}^4I_{9/2}$ transition (see the inset of Figure 4a). Compared with the room temperature, the intensity of $^4F_{7/2} \rightarrow {}^4I_{9/2}$ and $^4F_{5/2} \rightarrow {}^4I_{9/2}$ transitions at 548 K increases 180 and 29 times,

https://doi.org/10.1021/acs.inorgchem.2c00432
Inorg. Chem. 2022, 61, 5425−5432

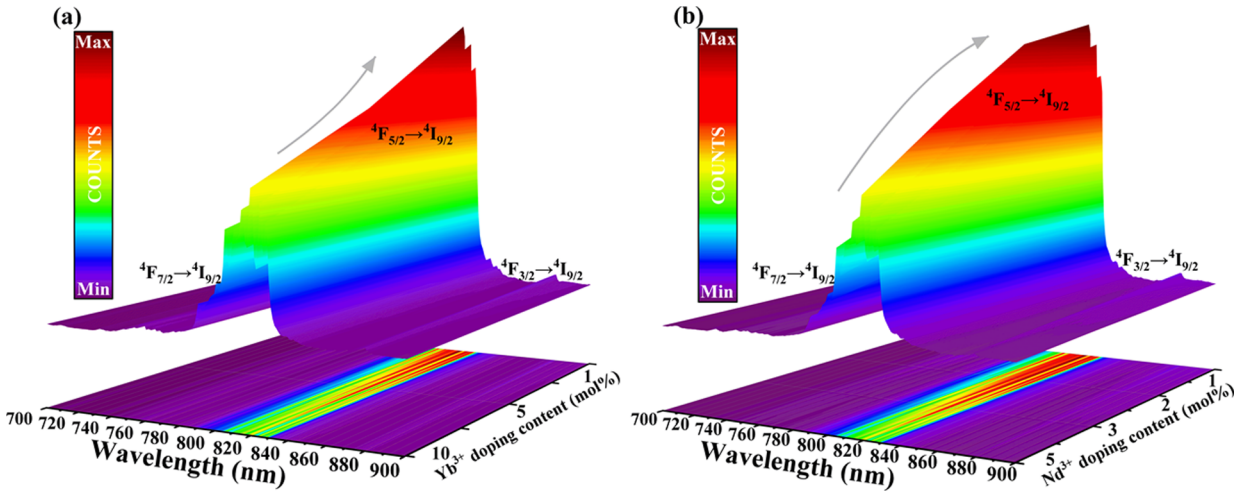

Figure 2. UC spectra of (a) BaY_2O_4: x % Yb^{3+}/1% Nd^{3+} (x = 1, 5, and 10) and (b) BaY_2O_4: 10% Yb^{3+}/y % Nd^{3+} (y = 1, 2, 3, and 5).

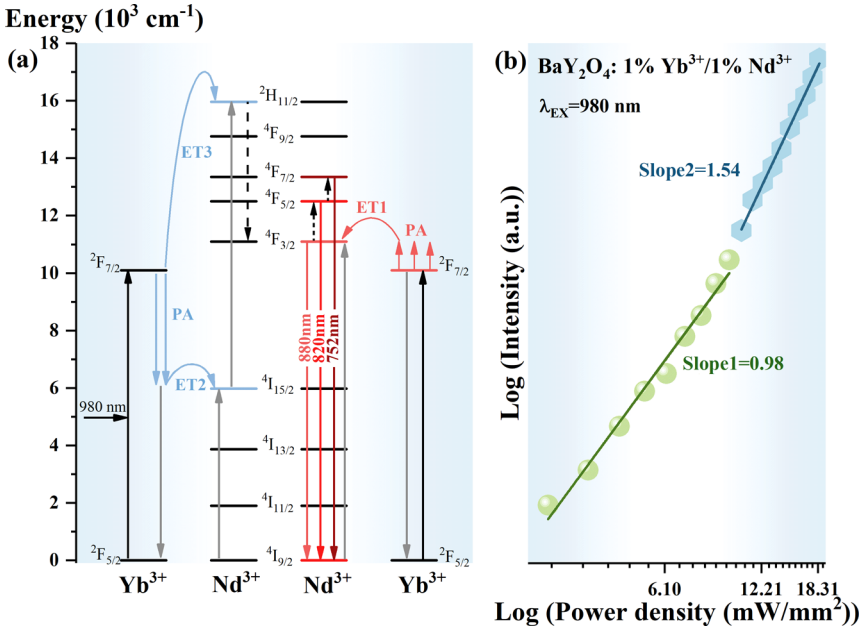

Figure 3. (a) Possible ET mechanisms in the Yb^{3+} and Nd^{3+} codoped system. (b) Log(I) − log(P) diagram of the $^4F_{5/2} \rightarrow {}^4I_{9/2}$ transition in BaY_2O_4: 1% Yb^{3+}/1% Nd^{3+}.

respectively, as shown in Figure 4b, which is partly attributed to the efficiency improvement of the PA ET processes between Yb^{3+} and Nd^{3+} benefiting from the intensification of lattice thermal vibration at high temperatures. In addition, the thermal population occurring from the low-lying state to the high-lying state of Nd^{3+} ions should be dramatically enhanced by raising the temperature, giving rise to the depopulation of the corresponding low-lying state. Ultimately, the $^4F_{7/2}$ level shows the largest thermal enhancement factor, followed by the $^4F_{5/2}$ level, and the $^4F_{3/2}$ level with a relatively small trend.

To shed more light on the thermally enhanced luminescence of the Nd^{3+}: ^4F_j (j = 7/2, 5/2, and 3/2) → $^4I_{9/2}$ transition, the lifetime curves of the Yb^{3+}: $^2F_{5/2}$ state in Yb^{3+} single-doped and Yb^{3+}/Nd^{3+} codoped samples at various temperatures are collected and the corresponding lifetimes are calculated, as plotted in Figures 5a,b and S1. With the increase in temperature, although the lifetimes of the Yb^{3+}: $^2F_{5/2}$ level in BaY_2O_4: 1% Yb^{3+} only show a slight decline, a distinct decrease in the lifetimes of the Yb^{3+}: $^2F_{5/2}$ level can be found in the Yb^{3+}/Nd^{3+} codoped sample. Whereafter, the ET rates ($W_{Yb\rightarrow Nd}$) between Yb^{3+} and Nd^{3+} at various temperatures are calculated by the following formula

$$W_{Yb\rightarrow Nd} = 1/\tau_{Yb\rightarrow Nd} - 1/\tau_{Yb} \quad (1)$$

where $\tau_{Yb\rightarrow Nd}$ and τ_{Yb} are the lifetime values of the Yb^{3+}: $^2F_{5/2}$ level in Yb^{3+}/Nd^{3+} codoped and Yb^{3+} singly doped BaY_2O_4, respectively.[36] As visualized in Figure 5b, the ET rate between Yb^{3+} and Nd^{3+} significantly increases from 0.15 ms^{-1} at 298 K to 0.32 ms^{-1} at 548 K with the increasing temperature, which is a compelling evidence for the thermally promoted ET processes from Yb^{3+} to Nd^{3+} with the assistance of phonons.

Considering the abundant metastable energy levels with small ΔE existing in Nd^{3+} ions, an effective light-to-heat conversion capacity can be anticipated to be obtained by a series of NR processes in BaY_2O_4: Yb^{3+}/Nd^{3+} powder. In order to verify this hypothesis, a 980 nm semiconductor laser is used for continuous irradiation on the present sample with an unchanged power density of 13.74 mW/mm^2, during which

https://doi.org/10.1021/acs.inorgchem.2c00432
Inorg. Chem. 2022, 61, 5425−5432

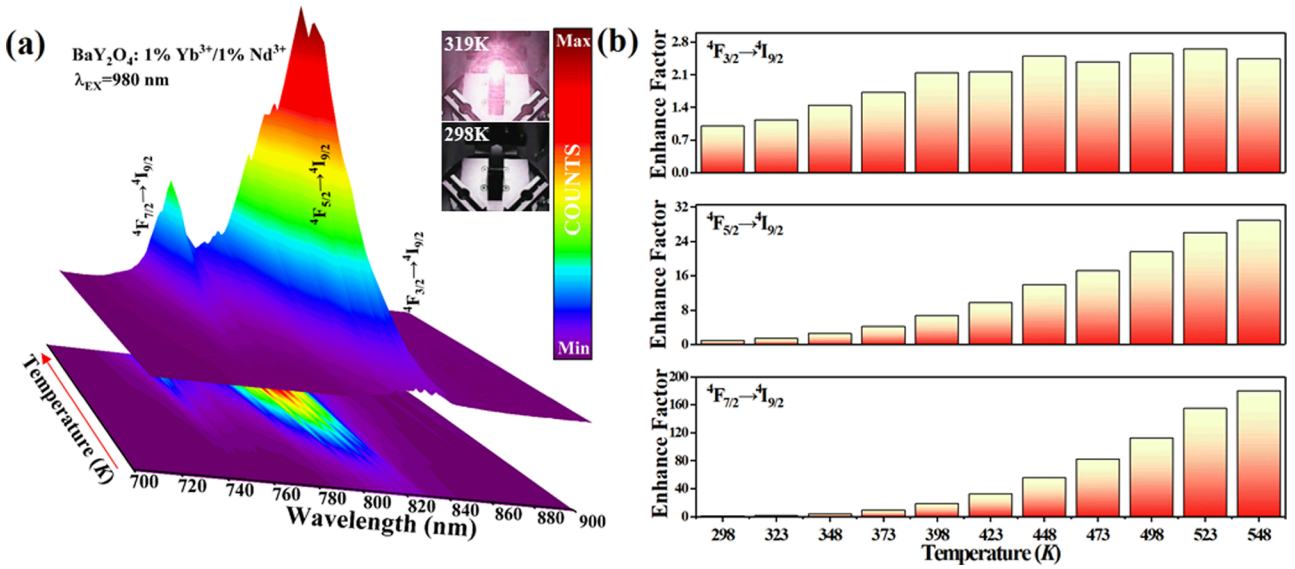

Figure 4. (a) Temperature-dependent spectra of BaY_2O_4: 1% Yb^{3+}/1% Nd^{3+} excited by 980 nm wavelength in the range of 298−548 K. The inset shows the luminescence images of the sample at 298 and 319 K taken using a thermal imager. (b) Enhance factor of the Nd^{3+}: ^4F_j (j = 7/2, 5/2, and 3/2) → $^4I_{9/2}$ transition at various temperatures.

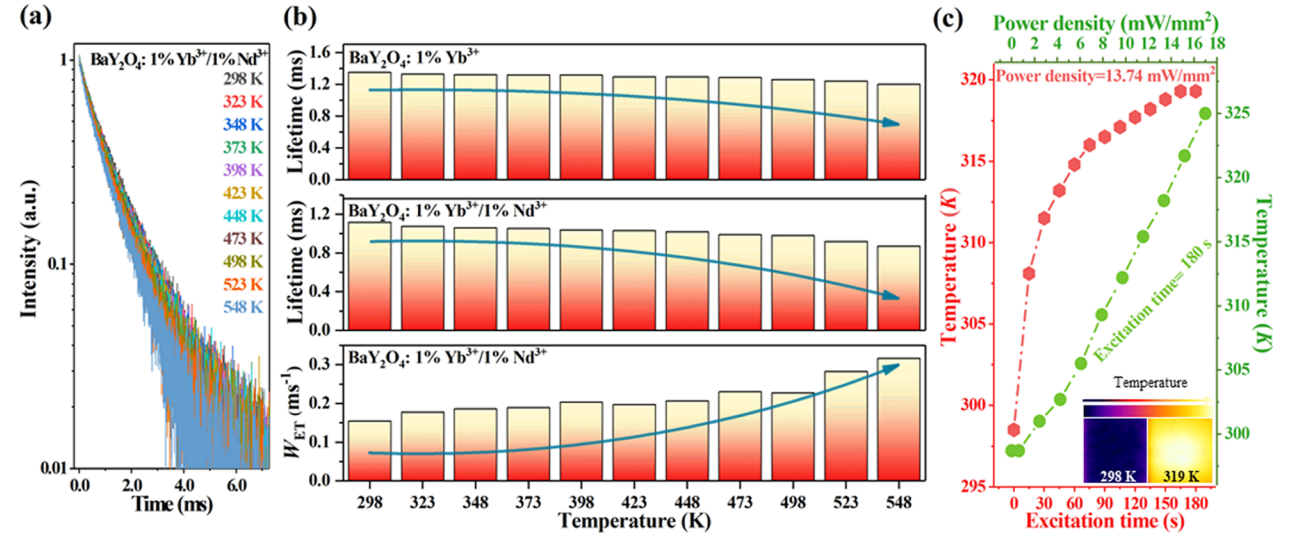

Figure 5. (a) Temperature dependence of lifetime curves of the Yb^{3+}: $^2F_{5/2}$ state in the BaY_2O_4: 1% Yb^{3+}/1% Nd^{3+} powder irradiated by 980 nm. (b) Calculated lifetimes of the Yb^{3+}: $^2F_{5/2}$ state in Yb^{3+} single-doped and Yb^{3+}/Nd^{3+} codoped samples and the corresponding ET rate between Yb^{3+} and Nd^{3+} at different temperatures. (c) Photothermal conversion effect of BaY_2O_4: 1% Yb^{3+}/1% Nd^{3+} as a function of irradiation duration and power density, respectively.

the temperature is monitored by IR thermography. As shown in Figure 5c, the sample temperature is gradually raised with the radiant time extension and comes up to its equilibrium temperature of 319.3 K after approximately 180 s, achieving an increase amplitude of 20.8 K, which is high enough to kill the cancer tissues during the PTT process.[37] Subsequently, the power density dependence of the photothermal conversion ability is also conducted with a constant radiant time of 180 s. Distinctly, the temperature of the sample increases monotonously with the increasing power density of 980 nm NIR light. The results mentioned above show the enormous potential of BaY_2O_4: Yb^{3+}/Nd^{3+} powder serving as an extraordinary photothermal conversion agent.

Optical Thermometry Behaviors. In order to discover the optical thermometry properties realized by the thermally coupled Nd^{3+}: ^4F_j (j = 7/2, 5/2, and 3/2) levels, the temperature-dependent luminescence spectra of BaY_2O_4: 1% Yb^{3+}/1% Nd^{3+} under the excitation of 980 nm are normalized to 1 at 820 nm, in which the intensity of the $^4F_{3/2}$ → $^4I_{9/2}$ transition is magnified by 10 times for better observation. As shown in Figure 6a, the relative emission intensities of the Nd^{3+}: ^4F_j (j = 7/2, 5/2, and 3/2) → $^4I_{9/2}$ transition show a regular variation with the increasing temperature, revealing its possibility for optical thermometry. Here, the FIR of $^4F_{7/2}$/$^4F_{5/2}$, $^4F_{5/2}$/$^4F_{3/2}$, and $^4F_{7/2}$/$^4F_{3/2}$ are denoted as TCL1, TCL2, and TCL3, respectively, which can be fitted by the Boltzmann distribution law

$$\mathrm{FIR} = I_2/I_1 = (\omega_2 A_2 g_2/\omega_1 A_1 g_1)\cdot\exp(-\Delta E/kT) = B\cdot\exp(-\Delta E/kT) \quad (2)$$

https://doi.org/10.1021/acs.inorgchem.2c00432
Inorg. Chem. 2022, 61, 5425−5432

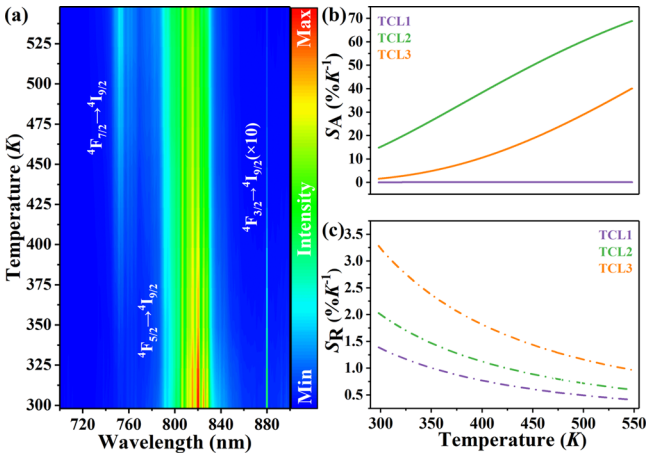

Figure 6. Temperature dependence of (a) emission spectra, (b) absolute sensitivity S_A, and (c) relative sensitivity S_R of BaY_2O_4: 1% Yb^{3+}/1% Nd^{3+} excited by 980 nm wavelength.

where I, A, ω, g, T, k, and B represent the emission intensity, spontaneous emission rate, angular frequency, degeneracy, absolute temperature, Boltzmann's constant, and a temperature-independent constant, respectively.[38−43] The corresponding FIR fitting curves are presented in Figure S2, from which the ΔE values are calculated to be 858 cm^{-1} ($^4F_{7/2}/^4F_{5/2}$), 1252 cm^{-1} ($^4F_{5/2}/^4F_{3/2}$), and 2022 cm^{-1} ($^4F_{7/2}/^4F_{3/2}$) for TCL1, TCL2, and TCL3 respectively.

As the important parameters of the optical thermometer, the fitting curves of the absolute sensitivity S_A and relative sensitivity S_R are outlined by the following equations

$$S_A = |d(FIR)/dT| = FIR\cdot\Delta E/(k_B\cdot T^2) \quad (3)$$

$$S_R = |d(FIR)/(FIR)\cdot dT| = \Delta E/(k_B\cdot T^2) \quad (4)$$

As shown in Figure 6b, the S_A values of TCL1, TCL2, and TCL3 increased with the rising temperature and reached their corresponding maximal values of 0.15, 68.88^{-}, and 40.13% K^{-1} at 548 K, respectively. On the contrary, the S_R values of TCL1, TCL2, and TCL3 decreased with the increasing temperature and reached their corresponding maximum values of 1.39, 2.03, and 3.29% K^{-1} at the initial temperature, respectively, as illustrated in Figure 6c. Utilizing the obtained S_A and S_R values, we can quantitatively compare the temperature sensing performance of BaY_2O_4: 1% Yb^{3+}/1% Nd^{3+} with others. Table 1 enumerates a series of temperature sensing materials based on the thermally coupled Nd^{3+}: ^4F_j (j = 7/2, 5/2, and 3/2) level, from which it can be seen that the present sample owns the highest absolute sensitivity S_A and its relative sensitivity S_R is only slightly less than that of oxygen fluorine glass, indicating the excellent optical thermometry ability of BaY_2O_4: Yb^{3+}/Nd^{3+}. Moreover, the accuracy of the present optical thermometer is evaluated by a self-designed experiment in which a heat gun is employed to heat the sample, and its temperature is determined by an IR temperature monitor and the FIR technology. As shown in Figure S3, the temperature calculated by FIR technology matches well with that detected using the IR thermometer, especially TCL3, with a maximum absolute error of 3 K. In addition, the FIR values of TCL1, TCL2, and TCL3 remained almost unchanged after conducting five cyclic processes, revealing their outstanding reproducibility for optical thermometry, as depicted in Figure S4.

Ex Vivo Examinations in Biotissues. A simple ex vivo test is devised to estimate the penetration depth of the Nd^{3+}: ^4F_j (j = 7/2, 5/2, and 3/2) → $^4I_{9/2}$ transition in BaY_2O_4: 1% Yb^{3+}/1% Nd^{3+}, as illustrated in Figure 7a. The collected spectra shown in Figure 7b are all measured at the ambient temperature. Distinctly, the far-red and NIR luminescence of Nd^{3+} is gradually decreased with the thickened chicken muscle tissues. However, the spectral profile remains almost unchanged with the adding thickness of the biological tissues. Moreover, its spectral information can still be gathered under 7 mm-thick biotissue due to the weak absorption and scattering effect of the biological tissues in this region, portending its potential application in the deep tissues.

CONCLUSIONS

In summary, a newfashioned photothermal conversion agent BaY_2O_4: Yb^{3+}/Nd^{3+} integrating with real-time temperature

Table 1. Various Nd^{3+}-Based Optical Thermometers with Related Parameters

materials	dopant	EX	TCLs	wavelength (nm)	T (K)	ΔE (cm^{-1})	S_R (K^{-1})	S_A (% K^{-1})	ref.
BaY_2O_4	Yb^{3+}/Nd^{3+}	980 nm	$^4F_{7/2}$, $^4F_{5/2}$	700−900	298−548	858	$1234/T^2$	0.15	this work
			$^4F_{5/2}$, $^4F_{3/2}$	700−900	298−548	1252	$1800/T^2$	68.88	this work
			$^4F_{7/2}$, $^4F_{3/2}$	700−900	298−548	2022	$2908/T^2$	40.13	this work
$LaPO_4$	Yb^{3+}/Nd^{3+}	980 nm	$^4F_{7/2}$, $^4F_{5/2}$	700−900	280−490	938	$1349/T^2$	0.11	21
			$^4F_{5/2}$, $^4F_{3/2}$	700−900	280−490	935	$1345/T^2$	18.53	21
			$^4F_{7/2}$, $^4F_{3/2}$	700−900	280−490	1897	$2727/T^2$	7.36	21
oxyfluoride glass	Yb^{3+}/Nd^{3+}	980 nm	$^4F_{7/2}$, $^4F_{5/2}$	720−900	303−623	1300	$1763/T^2$		36
			$^4F_{5/2}$, $^4F_{3/2}$	720−900	303−623	1216	$1884/T^2$		36
			$^4F_{7/2}$, $^4F_{3/2}$	720−900	303−623	2076	$3010/T^2$		36
La_2O_3	Yb^{3+}/Nd^{3+}	980 nm	$^4F_{7/2}$, $^4F_{5/2}$	725−850	293−1233	927	$1344/T^2$	0.03	38
$CaWO_4$	Yb^{3+}/Nd^{3+}/Li^+	980 nm	$^4F_{7/2}$, $^4F_{5/2}$	700−950	303−773	839	$1207/T^2$	0.01	44
			$^4F_{5/2}$, $^4F_{3/2}$	700−950	303−773	865	$1244/T^2$	0.39	44
			$^4F_{7/2}$, $^4F_{3/2}$	700−950	303−773	1722	$2476/T^2$	0.36	44
$Bi_4Ti_3O_{12}$	Yb^{3+}/Nd^{3+}	980 nm	$^4F_{7/2}$, $^4F_{5/2}$	700−850	323−573	867.2	$1248/T^2$	9.9	45
			$^4F_{7/2}$, $^4F_{5/2}$	720−950	297−420	889	$1288/T^2$		46
$NaYF_4$	Yb^{3+}/Nd^{3+}	980 nm	$^4F_{5/2}$, $^4F_{3/2}$	720−950	297−420	713	$1033/T^2$		46
			$^4F_{7/2}$, $^4F_{3/2}$	720−950	297−420	1433	$2076/T^2$		46

https://doi.org/10.1021/acs.inorgchem.2c00432
Inorg. Chem. 2022, 61, 5425−5432

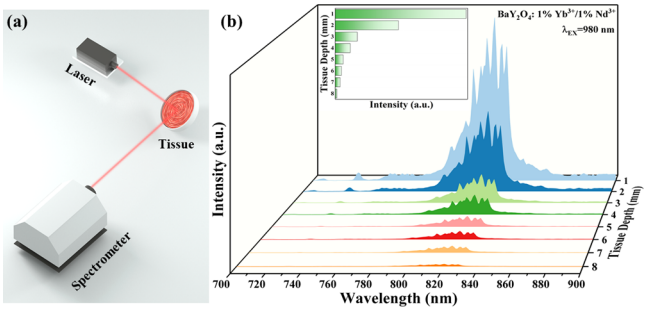

Figure 7. (a) Diagrammatic sketch of the ex vivo examination conducted at room temperature. (b) Biotissue thickness-dependent luminescence spectra of BaY_2O_4: 1% Yb^{3+}/1% Nd^{3+} under the excitation of 980 nm along with the corresponding integral intensity.

sensing has been designed successfully, which can be used for deep-tissue treatment because of the excitation and emission wavelengths located in the biological window. The optical thermometry behavior is based on the FIR of the thermally coupled Nd^{3+}: ^4F_j (j = 7/2, 5/2, and 3/2) level with the maximum S_A and S_R of 68.88 and 3.29% K^{-1}, respectively. More importantly, the emission intensity of the Nd^{3+} ion is significantly enhanced by increasing the temperature due to the improvement of PA ET efficiency, allowing the acquisition of a better signal-to-noise ratio during the temperature detection process. Meanwhile, the present sample shows remarkable photothermal conversion performance under the irradiation of 980 nm. The sample temperature can be raised to 319.3 K after 180 s of NIR irradiation with a fixed power density of 13.74 mW/mm^2, which is effective enough to destroy the pathological tissues. In addition, the penetration depth of the prepared sample in the biotissues was determined to be approximately 7 mm through a simple ex vivo examination. The abovementioned experimental data indicate that BaY_2O_4: Yb^{3+}/Nd^{3+} is a promising photothermal conversion agent equipped with an accurate temperature sensing function, which can be utilized in the deep-tissue PTT process.

■ ASSOCIATED CONTENT

Supporting Information

The Supporting Information is available free of charge at https://pubs.acs.org/doi/10.1021/acs.inorgchem.2c00432.

Temperature dependence of decay curves of the Yb^{3+}: $^2F_{5/2}$ level, temperature-dependent FIR curves, temperature of the sample obtained using an IR thermometer and FIR technology, and repeatability studies of TCL1, TCL2, and TCL3 (PDF)

■ AUTHOR INFORMATION

Corresponding Authors

Guotao Xiang − *Department of Mathematics and Physics, Chongqing University of Posts and Telecommunications, Chongqing 400065, China;* orcid.org/0000-0003-3587-6654; Email: xianggt@cqupt.edu.cn

Xiaojun Wang − *Department of Physics & Astronomy, Georgia Southern University, Statesboro, Georgia 30460, United States;* orcid.org/0000-0003-1506-0762; Email: xwang@georgiasouthern.edu

Jiahua Zhang − *State Key Laboratory of Luminescence and Applications, Changchun Institute of Optics, Fine Mechanics and Physics, Chinese Academy of Sciences, Changchun 130033, China;* Email: zhangjh@ciomp.ac.cn

Authors

Menglin Yang − *Department of Mathematics and Physics, Chongqing University of Posts and Telecommunications, Chongqing 400065, China*

Zhen Liu − *Department of Mathematics and Physics, Chongqing University of Posts and Telecommunications, Chongqing 400065, China*

Yongjie Wang − *Department of Mathematics and Physics, Chongqing University of Posts and Telecommunications, Chongqing 400065, China;* orcid.org/0000-0002-5580-8555

Sha Jiang − *Department of Mathematics and Physics, Chongqing University of Posts and Telecommunications, Chongqing 400065, China*

Xianju Zhou − *Department of Mathematics and Physics, Chongqing University of Posts and Telecommunications, Chongqing 400065, China;* orcid.org/0000-0002-8050-9688

Li Li − *Department of Mathematics and Physics, Chongqing University of Posts and Telecommunications, Chongqing 400065, China;* orcid.org/0000-0003-1163-5733

Li Ma − *Department of Physics & Astronomy, Georgia Southern University, Statesboro, Georgia 30460, United States*

Complete contact information is available at: https://pubs.acs.org/10.1021/acs.inorgchem.2c00432

Notes

The authors declare no competing financial interest.

■ ACKNOWLEDGMENTS

This work is financially supported by the National Natural Science Foundation of China (11704054, 11874055, 12004061, and 12004062) and the Science and Technology Research Program of Chongqing Municipal Education Commission (KJZD-K201800602 and KJZD-M202000601).

■ REFERENCES

(1) Xiang, G.; Xia, Q.; Liu, X.; Wang, Y.; Jiang, S.; Li, L.; Zhou, X.; Ma, L.; Wang, X.; Zhang, J. Upconversion nanoparticles modified by Cu_2S for photothermal therapy along with real-time optical thermometry. *Nanoscale* **2021**, *13*, 7161−7168.

(2) Vu, D. T.; Tsai, Y.-C.; Le, Q. M.; Kuo, S.-W.; Lai, N. D.; Benisty, H.; Lin, J.-Y.; Kan, H.-C.; Hsu, C.-C. A Synergy Approach to Enhance Upconversion Luminescence Emission of Rare Earth Nanophosphors with Million-Fold Enhancement Factor. *Crystals* **2021**, *11*, 1187.

(3) Suo, H.; Zhao, X.; Zhang, Z.; Wu, Y.; Guo, C. Up-converting $LuVO_4$: Nd^{3+}/Yb^{3+}/Er^{3+}@SiO_2 @Cu_2S hollow nanoplatforms for self-monitored photothermal ablation. *ACS Appl. Mater. Interfaces* **2018**, *10*, 39912−39920.

(4) Wiesholler, L. M.; Frenzel, F.; Grauel, B.; Würth, C.; Resch-Genger, U.; Hirsch, T. Yb, Nd, Er-Doped Upconversion Nanoparticles: 980 nm versus 808 nm Excitation. *Nanoscale* **2019**, *11*, 13440−13449.

(5) Suo, H.; Zhao, X.; Zhang, Z.; Shi, R.; Wu, Y.; Xiang, J.; Guo, C. Local symmetric distortion boosted photon up-conversion and thermometric sensitivity in lanthanum oxide nanospheres. *Nanoscale* **2018**, *10*, 9245−9251.

(6) Ansari, A. A.; Parchur, A. K.; Nazeeruddin, M. K.; Tavakoli, M. M. Luminescent lanthanide nanocomposites in thermometry: chemistry of dopant ions and host matrices. *Coord. Chem. Rev.* **2021**, *444*, 214040.

(7) Golyeva, E. V.; Kalinichev, A. A.; Landeranta, E.; Mikhailov, M. Nd3+ single doped YVO4 nanoparticles for sub-tissue heating and thermal sensing in the second biological window. *Sens. Actuators, B* **2017**, *243*, 338−345.
(8) Liu, X.; Li, T.; Zhao, X.; Suo, H.; Zhang, Z.; Zhao, P.; Gao, S.; Niu, M. 808 nm-triggered optical thermometry based on up-conversion luminescence of $Nd^{3+}/Yb^{3+}/Er^{3+}$ doped MIn_2O_4 (m = Ca, Sr and Ba) phosphors. *Dalton Trans.* **2018**, *47*, 6713−6721.
(9) Zhou, Y.; Cheng, Y.; Huang, Q.; Xu, J.; Lin, H.; Wang, Y. Abnormal thermally enhanced upconversion luminescence of lanthanide-doped phosphors: proposed mechanisms and potential applications. *J. Mater. Chem. C* **2021**, *9*, 2220−2230.
(10) Zhou, Y.; Cheng, Y.; Xu, J.; Lin, H.; Wang, Y. Thermo-enhanced upconversion luminescence in inert-core/active-shell UCNPs: the inert core matters. *Nanoscale* **2021**, *13*, 6569−6576.
(11) Zhang, N.; Molokeev, M. S.; Liu, Q.; Xia, Z. Pure red upconversion luminescence and optical thermometry of Er^{3+} doped sensitizer-rich $SrYbInO_4$ phosphors. *J. Mater. Chem. C* **2018**, *6*, 7361−7366.
(12) Liu, P.; Liu, J.; Zhang, Y.; Xia, Z.; Xu, Y. Morphology controlled synthesis of $Ba_4Bi_3F_{17}$: Er^{3+}, Yb^{3+} and the dual-functional temperature sensing and optical heating applications. *J. Alloys Compd.* **2020**, *844*, 156116.
(13) Yu, Z.; Xia, Z.; Liu, E.; Liu, Q. Synthesis, up-conversion luminescence and thermometry of Yb^{3+}/Er^{3+} co-doped $La_{2.4}Mo_{1.6}O_8$ phosphors. *Dalton Trans.* **2016**, *45*, 16240−16245.
(14) Liu, K.-C.; Zhang, Z.-Y.; Shan, C.-X.; Feng, Z.-Q.; Li, J.-S.; Song, C.-L.; Bao, Y.-N.; Qi, X.-H.; Dong, B. A flexible and superhydrophobic upconversion-luminescence membrane as an ultrasensitive fluorescence sensor for single droplet detection. *Light: Sci. Appl.* **2016**, *5*, No. e16136.
(15) Zhang, J.; Hao, Z.; Li, J.; Zhang, X.; Luo, Y.; Pan, G. Observation of efficient population of the red-emitting state from the green state by non-multiphonon relaxation in the Er^{3+}-Yb^{3+} system. *Light: Sci. Appl.* **2015**, *4*, No. e239.
(16) Zhang, X.; Gao, R.; Wang, Z.; Zhang, Y.; Hu, Y.; Sun, L.; Fu, L.; Ai, X.-C.; Zhang, J.-P. Effect of excitation mode on the upconversion luminescence of β-$NaYF_4$: Yb/Er nanocrystals. *Chem. Phys. Lett.* **2021**, *779*, 138880.
(17) Wang, F.; Liu, X. Recent advances in the chemistry of lanthanide-doped upconversion nanocrystals. *Chem. Soc. Rev.* **2009**, *38*, 976−989.
(18) Auzel, F. Upconversion and anti-stokes processes with f and d ions in solids. *Chem. Rev.* **2004**, *104*, 139−174.
(19) Zhu, X.; Feng, W.; Chang, J.; Tan, Y.-W.; Li, J.; Chen, M.; Sun, Y.; Li, F. Temperature-feedback upconversion nanocomposite for accurate photothermal therapy at facile temperature. *Nat. Commun.* **2016**, *7*, 10437.
(20) Rodríguez-Sevilla, P.; Zhang, Y.; Haro-González, P.; Sanz-Rodríguez, F.; Jaque, F.; Solé, J. G.; Liu, X.; Jaque, D. Thermal scanning at the cellular level by an optically trapped upconverting fluorescent particle. *Adv. Mater.* **2016**, *28*, 2421−2426.
(21) Suo, H.; Zhao, X.; Zhang, Z.; Guo, C. Ultra-sensitive optical nano-thermometer $LaPO_4$: Yb^{3+}/Nd^{3+} based on thermo-enhanced NIR-to-NIR emissions. *Chem. Eng. J.* **2020**, *389*, 124506.
(22) Ye, Z.-Q.; Xiao, S.-G.; Yang, X.-L. Up-conversion of $Nd^{3+}/Yb^{3+}/Tm^{3+}$ tri-doped $CaTeO_3$ compound under excitation of 808 nm. *Rare Met.* **2021**, *40*, 1008−1013.
(23) Zheng, X.; Kankala, R. K.; Liu, C.-G.; Wang, S.-B.; Chen, A.-Z.; Zhang, Y. Lanthanides-doped near-infrared active upconvert-sion nanocrystals: Upconversion mechanisms and synthesis. *Coord. Chem. Rev.* **2021**, *438*, 213870.
(24) Kalinichev, A. A.; Kurochkin, M. A.; Golyeva, E. V.; Kurochkin, A. V.; Lähderanta, E.; Mikhailov, M. D.; Kolesnikov, I. E.; Kolesnikov, I. E. Near-infrared emitting YVO_4:Nd^{3+} nanoparticles for high sensitive fluorescence thermometry. *J. Lumin.* **2018**, *195*, 61−66.
(25) Song, N.; Liu, S.; Zhang, P.; He, J.; Zhang, Q.; Wang, F.; Zhou, B. Enhancing upconversion of Nd^{3+} through Yb^{3+}- mediated energy cycling towards temperature sensing. *J. Rare Earths* **2021**, *39*, 1506−1511.
(26) Pokhrel, M.; Valdes, C.; Mao, Y. Ultraviolet upconversion enhancement in triply doped $NaYF_4$: Tm^{3+}, Yb^{3+} particles: The role of Nd^{3+} or Gd^{3+} Co-doping. *Opt. Mater.* **2016**, *58*, 67−75.
(27) Ji, Y.; Xu, W.; Ding, N.; Yang, H.; Song, H.; Liu, Q.; Ågren, H.; Widengren, J.; Liu, H. Huge upconversion luminescence enhancement by a cascade optical field modulation strategy facilitating selective multispectral narrow-band near-infrared photodetection. *Light: Sci. Appl.* **2020**, *9*, 184.
(28) Wang, F.; Wen, S.; He, H.; Wang, B.; Zhou, Z.; Shimoni, O.; Jin, D. Microscopic inspection and tracking of single upconversion nanoparticles in living cells. *Light: Sci. Appl.* **2018**, *7*, 18007.
(29) Dianov, E. M.; Evgeny, M. Bismuth-doped optical fibers: a challenging active medium for near-IR lasers and optical amplifiers. *Light: Sci. Appl.* **2012**, *1*, No. e12.
(30) Song, N.; Zhou, B.; Yan, L.; Huang, J.; Zhang, Q. Understanding the Role of Yb^{3+} in the Nd/Yb Coupled 808-nm-Responsive Upconversion. *Front. Chem.* **2019**, *6*, 673.
(31) Wang, D.; Xue, B.; Song, J.; Qu, J. Compressed energy transfer distance for remarkable enhancement of the luminescence of Nd^{3+}-sensitized upconversion nanoparticles. *J. Mater. Chem. C* **2018**, *6*, 6597−6604.
(32) Wang, T.; Zhou, H.; Yu, Z.; Zhou, G.; Zhou, J.; Huang, D.; Sun, L.; Gao, P.; Sun, Y.; Hu, J. 808 nm excited multicolor upconversion tuning through energy migration in core−shell−shell nanoarchitecture. *J. Phys. Chem. C* **2018**, *122*, 10113−10124.
(33) Yang, Z.; Zhao, Y.; Zhou, Y.; Qiao, J.; Chuang, Y. C.; Molokeev, M. S.; Xia, Z. Giant red-shifted emission in $(Sr,Ba)Y_2O_4$: Eu^{2+} phosphor toward broadband near-infrared luminescence. *Adv. Funct. Mater.* **2022**, *32*, 2103927.
(34) Xiang, G.; Liu, X.; Xia, Q.; Jiang, S.; Zhou, X.; Li, L.; Jin, Y.; Ma, L.; Wang, X.; Zhang, J. Deep-tissue temperature sensing realized in BaY_2O_4: Yb^{3+}/Er^{3+} with ultrahigh sensitivity and extremely intense red upconversion luminescence. *Inorg. Chem.* **2020**, *59*, 11054−11060.
(35) Mi, C.; Zhou, J.; Wang, F.; Jin, D. Thermally enhanced NIR−NIR anti-stokes emission in rare earth doped nanocrystals. *Nanoscale* **2019**, *11*, 12547−12552.
(36) Xu, W.; Zhao, H.; Zhang, Z.; Cao, W. Highly sensitive optical thermometry through thermally enhanced near infrared emissions from Nd^{3+}/Yb^{3+} codoped oxyfluoride glass ceramic. *Sens. Actuators, B* **2013**, *178*, 520−524.
(37) Ximendes, E. C.; Rocha, U.; Jacinto, C.; Kumar, K. U.; Bravo, D.; López, F. J.; Rodríguez, E. M.; García-Solé, J.; Jaque, D. Self-monitored photothermal nanoparticles based on core−shell engineering. *Nanoscale* **2016**, *8*, 3057−3066.
(38) Gao, G.; Busko, D.; Kauffmann-Weiss, S.; Turshatov, A.; Howard, I. A.; Richards, B. S. Wide-range non-contact fluorescence intensity ratio thermometer based on Yb^{3+}/Nd^{3+} co-doped La_2O_3 microcrystals operating from 290 to 1230 K. *J. Mater. Chem. C* **2018**, *6*, 4163−4170.
(39) Jiang, S.; Zeng, P.; Liao, L.; Tian, S.; Guo, H.; Chen, Y.; Duan, C.; Yin, M. Optical thermometry based on upconverted luminescence in transparent glass ceramics containing $NaYF_4$: Yb^{3+}/Er^{3+} nanocrystals. *J. Alloys Compd.* **2014**, *617*, 538−541.
(40) Xiang, G.; Xia, Q.; Liu, X.; Wang, X. Optical thermometry based on the thermally coupled energy levels of Er^{3+} in upconversion materials. *Dalton Trans.* **2020**, *49*, 17115.
(41) Kolesnikov, I. E.; Mamonova, D. V.; Kalinichev, A. A.; Kurochkin, M. A.; Medvedev, V. A.; Kolesnikov, E. Y.; Lähderanta, E.; Manshina, A. A. Constructing of efficient dual activating ratiometric YVO_4: Nd^{3+}/Eu^{3+} nanothermometer: co-doping or mixture. *Nanoscale* **2020**, *12*, 5953−5960.
(42) Cao, B.; Bao, Y.; Liu, Y.; Shang, J.; Zhang, Z.; He, Y.; Feng, Z.; Dong, B. Wide-range and highly- sensitive optical thermometers based on the temperature-dependent energy transfer from Er to Nd in Er/Yb/Nd codoped $NaYF_4$ upconversion nanocrystals. *Chem. Eng. J.* **2020**, *385*, 123906.

https://doi.org/10.1021/acs.inorgchem.2c00432
Inorg. Chem. 2022, 61, 5425−5432

(43) Wade, S. A.; Collins, S. F.; Baxter, G. W. Fluorescence intensity ratio technique for optical fiber point temperature sensing. *J. Appl. Phys.* **2003**, *94*, 4743−4756.
(44) Xu, W.; Hu, Y.; Zheng, L.; Zhang, Z.; Cao, W.; Liu, H.; Wu, X. Enhanced nir-nir luminescence from $CaWO_4$: Nd^{3+}/Yb^{3+} phosphors by Li^+ codoping for thermometry and optical heating. *J. Lumin.* **2019**, *208*, 415−423.
(45) Chen, H.; Bai, G.; Yang, Q.; Hua, Y.; Xu, S.; Chen, L. Non-contact fluorescence intensity ratio optical thermometer based on Yb^{3+}/Nd^{3+} codoped $Bi_4Ti_3O_{12}$ microcrystals. *J. Lumin.* **2020**, *221*, 117095.
(46) Xu, W.; Qi, H.; Zheng, L.; Zhang, Z.; Cao, W. Multifunctional nanoparticles based on the Nd^{3+}/Yb^{3+} codoped $NaYF_4$. *Opt. Lett.* **2015**, *40*, 5678.

https://doi.org/10.1021/acs.inorgchem.2c00432
Inorg. Chem. 2022, 61, 5425−5432